Interdecadal Variations of Meridional Winds in the South China Sea and Their Relationship with Summer Climate in China*

CHUNHUI LI

Key Open Laboratory for Tropical Monsoon, Institute of Tropical and Marine Meteorology, China Meteorological Administration, Guangzhou, China

TIM LI

International Pacific Research Center, and Department of Meteorology, University of Hawaii at Manoa, Honolulu, Hawaii

JIANYIN LIANG, DEJUN GU, AILAN LIN, AND BIN ZHENG

Key Open Laboratory for Tropical Monsoon, Institute of Tropical and Marine Meteorology, China Meteorological Administration, Guangzhou, China

(Manuscript received 31 July 2008, in final form 2 July 2009)

ABSTRACT

Analysis of the NCEP and 40-yr ECMWF Re-Analysis (ERA-40) data and the Xisha Island station observation indicates that the low-level meridional wind (LLMW) over the South China Sea (SCS) experienced an interdecadal variation since the late 1970s. The LLMW change is associated with the reduction of tropospheric temperature in midlatitude East Asia. A mechanism is put forward to explain the triggering and maintenance of the tropospheric cooling. The enhanced convective heating over the southern South China Sea results in a meridional vertical overturning circulation, with anomalous descending motion appearing over continental East Asia. The anomalous descending motion reduces the local humidity through both anomalous low-level divergence and dry vertical advection. The decrease of the local tropospheric humidity leads to the enhanced outgoing longwave radiation into space and thus cold temperature anomalies. The decrease of the temperature and thickness leads to anomalous low (high) pressure and convergent (divergent) flows at upper (lower) levels. This further enhances the descending motion and leads to a positive feedback loop.

The fall in tropospheric temperature over continental East Asia reduces the land–sea thermal contrast and leads to the weakening of cross-equatorial flows and the LLMW over SCS. A further diagnosis indicates that the LLMW is closely linked to the summer precipitation and temperature variations in China on interdecadal time scales. A weakening of the LLMW after 1976 is associated with a "−, +, −" meridional rainfall pattern, with less rain in Guangdong Province and north China but more rain in the Yangtze and Huaihe River basins and northeast China, and a "+, −, +" temperature pattern, with increased (decreased) surface temperature in the south and north (central) China.

1. Introduction

Significant interdecadal variations have taken place since the late 1970s in global atmospheric circulation and SST (Nitta and Yamada 1989; Wang 1995). As part of the global circulation, the East Asian monsoon also experienced a significant interdecadal variation (Li et al. 1999). For example, the summer precipitation increases significantly in the basin of the Yangtze River while severe droughts have been sustained over north China and along

* School of Ocean and Earth Science and Technology Contribution Number 7867 and International Pacific Research Center Contribution Number 661.

Corresponding author address: Chunhui Li, Key Open Laboratory for Tropical Monsoon, Institute of Tropical and Marine Meteorology, China Meteorological Administration, Guangzhou 510080, China.
E-mail: chli@grmc.gov.cn

DOI: 10.1175/2009JCLI2762.1

the Yellow River basin since the late 1970s (Huang et al. 1999; Huang 1999; Wang 2001, 2002). Introducing a land–sea surface pressure difference index, (Guo et al. 2003) showed that the intensity of the East Asian monsoon decreased significantly after the late 1970s. Physically, the teleconnection of the East Asian monsoon to El Niño is through an anomalous anticyclone over the western North Pacific (WNP) that persists from the mature phase of the El Niño to the subsequent summer through a positive local air–sea feedback (Wang et al. 2000). This Pacific–East Asia teleconnection, however, experiences a significant interdecadal change (Chang et al. 2000a,b). The cause of such an interdecadal change is argued to be related to the interdecadal variation of the SST anomaly (SSTA) in the tropical Pacific (Chang et al. 2000a,b; Huang 2001).

As a part of the East Asian summer monsoon system, the rainfall and circulation patterns in the South China Sea (SCS) exert a significant impact on the East Asian climate. After the onset of the SCS monsoon, water vapor originating from the SCS and tropical western Pacific is advected by the monsoon flows toward East Asia to maintain mei-yu and baiu during June and July (Murakami 1959). The ENSO-induced SSTA in the SCS tends to persist from boreal winter to the ensuing spring and summer (e.g., Lanzante 1996; Wang et al. 2000), impacting the monsoon rainfall in China (Shen and Lau 1995; Tomita and Yasunari 1996). The SCS summer monsoon experienced an abrupt interdecadal change in the late 1970s (Dai et al. 2000; Liang and Wu 2003). The weakening of the SCS monsoon is mainly caused by the significant decrease of southerly component of the low-level wind (Liang et al. 2007).

Unlike the Indian monsoon that has pronounced westerlies in association with a north–south thermal contrast between the heated Asian continent and cooled Indian Ocean, the East Asian monsoon is marked by dominant southerlies in association with the zonal pressure gradient between a continental thermal low and an oceanic cold high (Chen and Chen 1991; Li and He 2001; Li and Zhang 1999; Sun et al. 2002; Ren and Qian 2003). Thus the meridional wind component is one of the key variables that reflect the intensity of the East Asian monsoon.

In this study we intend to reveal the large-scale circulation and SST patterns and physical mechanisms associated with the interdecadal change of the low-level meridional wind (LLMW) over SCS. We will also reveal how the change of the LLMW is related to the summer climate in China and investigate the relative role of the zonal and meridional wind components over the SCS in contributing to the interannual and interdecadal variabilities of the East Asian climate. The rest of the paper is organized as follows: In section 2, we describe the data and methods used. The large-scale circulation and SST patterns associated with the SCS LLMW change are revealed and possible physical mechanisms that cause and maintain the midlatitude temperature and circulation anomalies are discussed in section 3. The relationship between the LLMW and summer precipitation and temperature over 743 weather stations across China is investigated in section 4. Finally, a summary and discussion are given in section 5.

2. Data and methods

To reduce the uncertainty in the reanalysis products, we use the ensemble mean of the National Centers for Environmental Prediction (NCEP) and 40-yr European Centre for Medium-Range Weather Forecasts (ECMWF) Re-Analysis (ERA-40) data. These global $2.5° \times 2.5°$ monthly mean reanalysis data consist of 12-layer temperature, geopotential height, and wind fields from 100 to 1000 hPa and four surface heat flux (i.e., latent and sensible heat flux and the net upward longwave and downward shortwave radiation) components for the period of 1958–2002. Other data used in this study include 1) precipitation and temperature data from 743 weather stations across China (1958–2002) provided by the National Climate Center of China, 2) Hadley Centre monthly mean SST data (HadISST; Rayner et al. 2003) at a $1° \times 1°$ horizontal resolution and the global ocean SST field from the Simple Ocean Data Assimilation (SODA; Carton and Giese 2008) at a $0.5° \times 0.5°$ horizontal resolution, and 3) the surface wind measured directly from the Xisha Islands (1958–98). The Xisha Islands are composed of a group of islands located over the central northern South China Sea. The data were observed at the Yongxing Island, the largest island of the group of coral islands. The Yongxing Island, with an area of about 2 km^2, is located at 16°50′N, 112°20′E. However, the observation station over Yongxing is officially referred to as the Xisha station.

The methods used in this study include the wavelet analysis, composite and correlation analyses, and the Mann–Kendal abrupt change test. The Mann–Kendall test (Magaritz and Goodfriend 1987) is a statistical verification method. It does not require a certain types of the sample distribution. For a smooth random series X_i $(1 \le i \le N)$, a statistical quantity of $\mathrm{UF}_k = [\mathrm{dk} - E(\mathrm{dk})]/[\sqrt{\mathrm{var}(\mathrm{dk})}]$ is constructed, where $\mathrm{dk} = \sum M_i$, M_i is the number of samples for which the value is smaller than X_i; that is, $M_i = \{X_j\colon j < i \text{ and } X_i < X_j\}$. Here $E(\mathrm{dk})$ is the mean and var(dk) is the variance. With the assumption of a randomly stable series, dk closely resembles a normal distribution, while UF_k has a standard normal distribution. The probability, as denoted

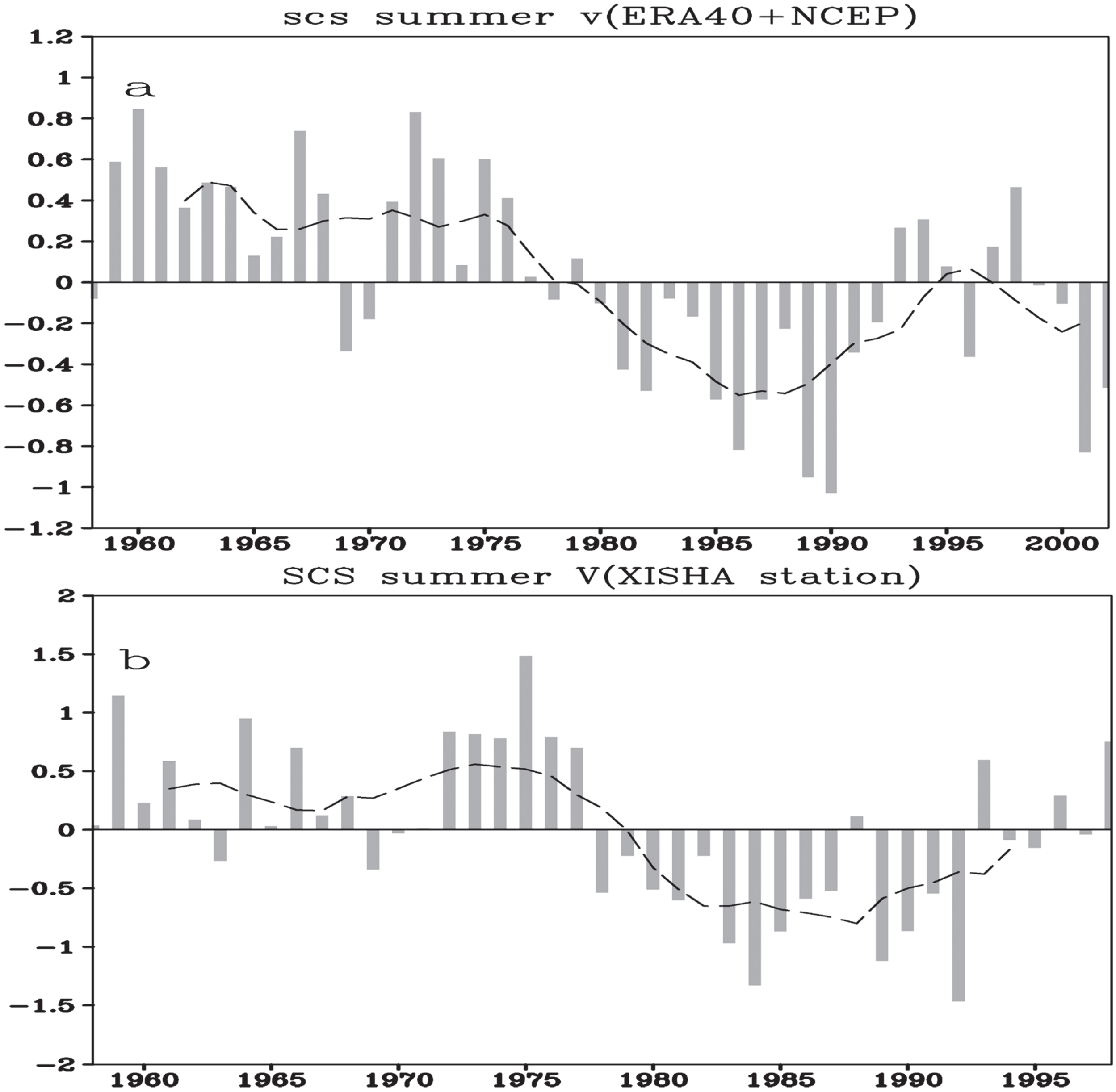

FIG. 1. Evolutions of (a) the area-averaged (5°–20°N, 105°–120°E) 850-hPa meridional wind (m s^{-1}) derived from the ensemble average of NCEP and ERA-40 reanalysis data and (b) the surface meridional wind measured directly from the Xisha station. The bars denote the averaged values in June–August (JJA) each year. The curves denote 9-yr running mean values.

by α, may be determined from a standard table. For a given significance level α_0, $\alpha > \alpha_0$ indicates a smooth stable series in which there is no significant turning point, and $\alpha < \alpha_0$ indicates that there is a turning point. As UF_k is calculated based on the original forward time series, a new quantity UB_k is calculated from a backward time series. When plotting both the curves, UF_k and UB_k, the intersection of the two curves within the confidence interval may be regarded as a turning point when an abrupt change appears.

3. Large-scale circulation and SST patterns associated with the interdecadal variation of LLMW over SCS

Figure 1a illustrates the evolution of the ensemble-averaged NCEP and ERA-40 850-hPa meridional wind anomaly averaged over SCS (5°–20°N, 105°–120°E) in boreal summer (June–August) from 1958 to 2002. A remarkable interdecadal shift of the LLMW has taken place since the late 1970s. Positive wind anomalies are

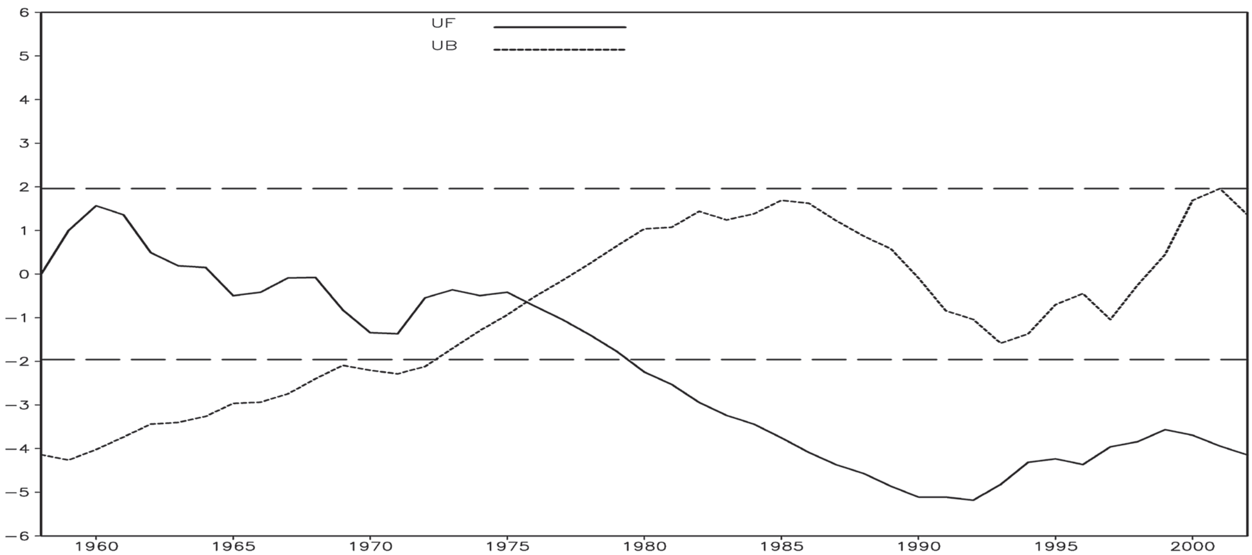

FIG. 2. Curves for abrupt change coefficients UF and UB, based on the time series of the 850-hPa meridional wind (m s^{-1}) averaged over SCS. The area between the two long dashed lines indicates that the abrupt changepoint exceeds the 95% confidence level.

predominant prior to this time and negative anomalies are predominant after it, indicating a change of intensity of the monsoon southerly from strong to weak. To examine the significance of this change, the Mann–Kendall test for abrupt change has been conducted, and the result is shown in Fig. 2. Note that the intensity of the LLMW weakens significantly, beyond the 0.05 significance level, after the late 1970s. The intersection of UF and UB curves appears in 1976, indicating that 1976 is the time of the abrupt change.

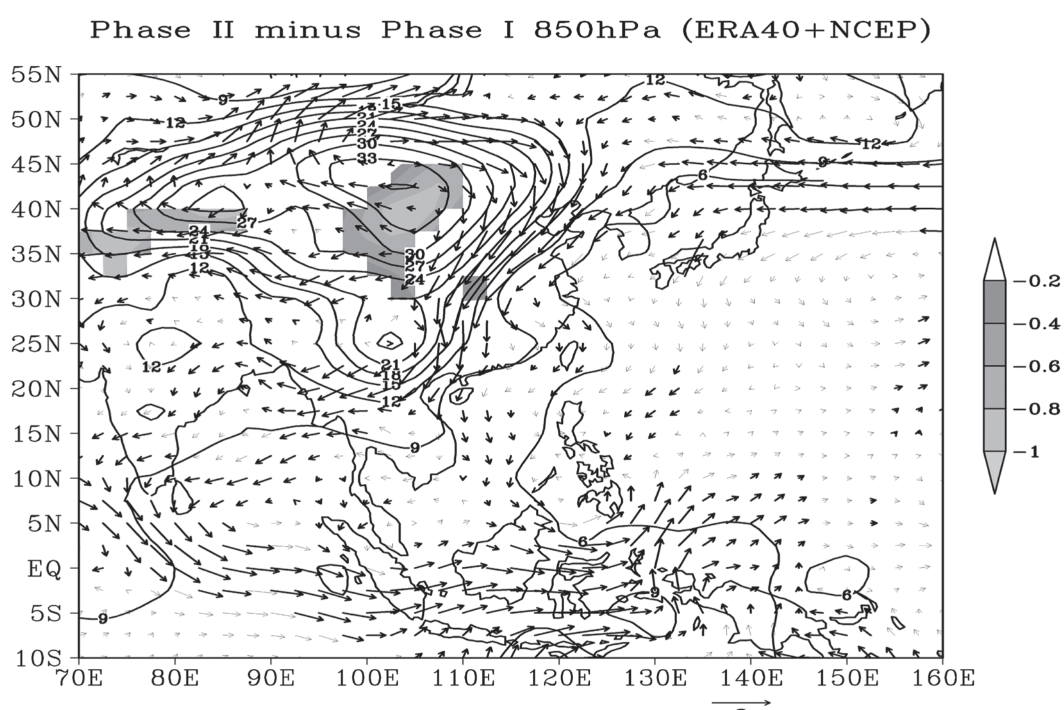

FIG. 3. The difference (phase II minus phase I) wind (vector; m s^{-1}; dark vectors denote that the difference exceeds the 95% confidence level), geopotential height (contour; gpm), and temperature (shaded; °C) fields at 850 hPa. A Student's t test is applied for examining the statistical significance. For the contour and shaded fields, only the differences that exceed the 95% confidence level (i.e., $t_\alpha = \pm 2.04$) are plotted.

To verify the reliability of the NCEP and ERA-40 reanalysis products, an independent dataset, directly measured from the surface observations at the Xisha Island station, is used. As shown in Fig. 1b, a similar evolution characteristic but with larger amplitude appears in the surface station observation. Again the Mann–Kendall test shows a significant abrupt change of the surface meridional wind at the end of the 1970s (figure not shown). Thus, the significant interdecadal change of the LLMW is found in both the island station observation and the NCEP–ERA-40 reanalysis.

A composite analysis is conducted to reveal the large-scale circulation and SST patterns associated with the interdecadal change of the LLMW over SCS. Here the data period is divided into two phases, with phase I being from 1960 to 1976 and phase II from 1980 to 2002. Figure 3 illustrates 850-hPa wind, geopotential height, and temperature difference (phase II minus phase I) fields. Note that negative temperature anomalies appear over midlatitude East Asia (35°–45°N). Associated with the significant cooling anomalies are positive geopotential height and anticyclonic circulation anomalies in the lower troposphere. The reduced land–sea thermal contrast weakens the East Asian monsoon and the low-level southerly flow over China. It also decreases the northward cross-equatorial flow over the longitudinal band of 80°–120°E.

The large-scale cooling at 850 hPa after 1976 over East Asia is at odds with the global warming trend. To illustrate the vertical structure of the temperature change, we plot area-averaged temperature profiles for phases I and II (Fig. 4a). Note that, since 1976, the temperature has fallen sharply throughout the troposphere. Correspondingly, the geopotential height and the meridional wind also show significant interdecadal variations (Figs. 4b,c), with the geopotential height rising and the meridional wind decreasing below 200 hPa after 1976.

A key issue is what causes the temperature drop at phase II. While the surface warming in tropical Pacific and Indian Oceans is quite remarkable since 1976, the changing trend of the temperature over the Eurasian continent differs significantly from season to season (Zeng and Yan 1999; Zeng et al. 2001). The cause of the tropospheric cooling over East Asia is speculated to be related to the eastward propagation of the cold temperature anomaly from western Europe in association with the strengthening of the North Atlantic Oscillation (NAO) (Yu and Zhou 2004; Zhou and Yu 2005; Yu et al. 2004; Xin et al. 2006).

Figure 5 illustrates the meridional–vertical section of difference (phase II minus phase I) fields for the temperature, geopotential height, zonal and meridional winds, and vertical velocity averaged between 100° and ~110°E. In the temperature difference field, the dominant pattern is negative anomalies in the midlatitude and weak positive anomalies in the tropics (Fig. 5a). The hydrostatic relation requires a positive (negative) geopotential

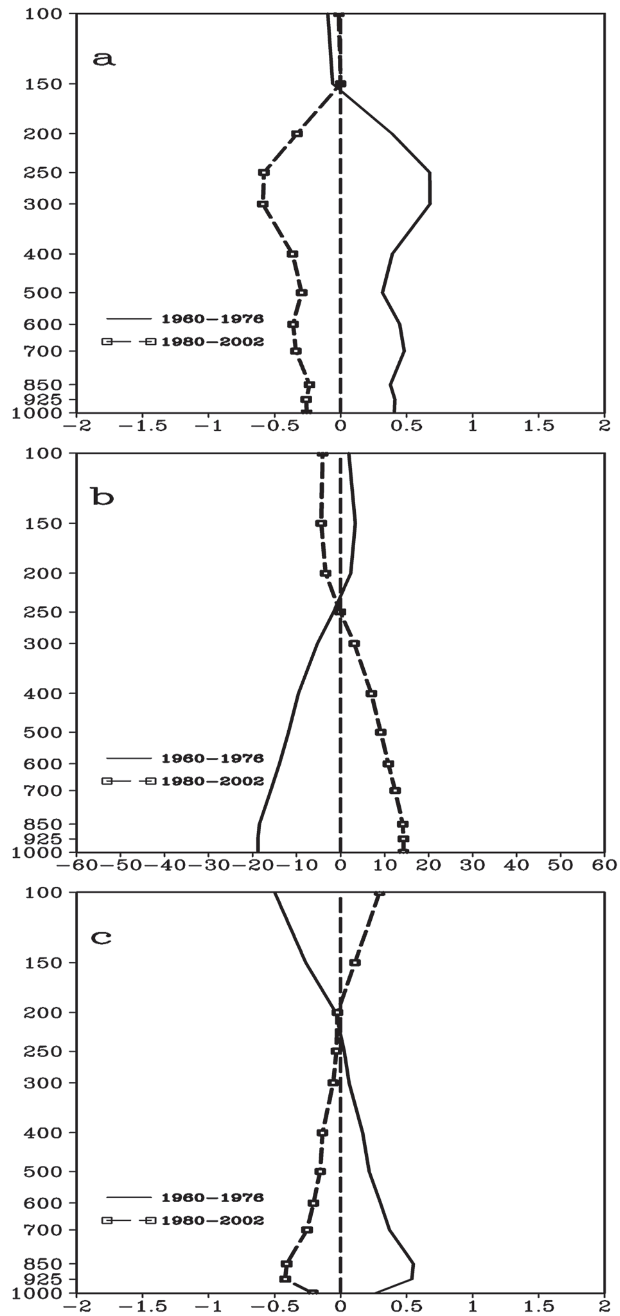

FIG. 4. Vertical profiles of (a) temperature (°C) and (b) geopotential height (gpm) anomalies averaged over 35°~45°N, 100°~110°E. (c) Meridional wind anomalies (m s^{-1}) averaged over 20°~30°N, 110°~120°E at phase I (solid line) and phase II (dashed line).

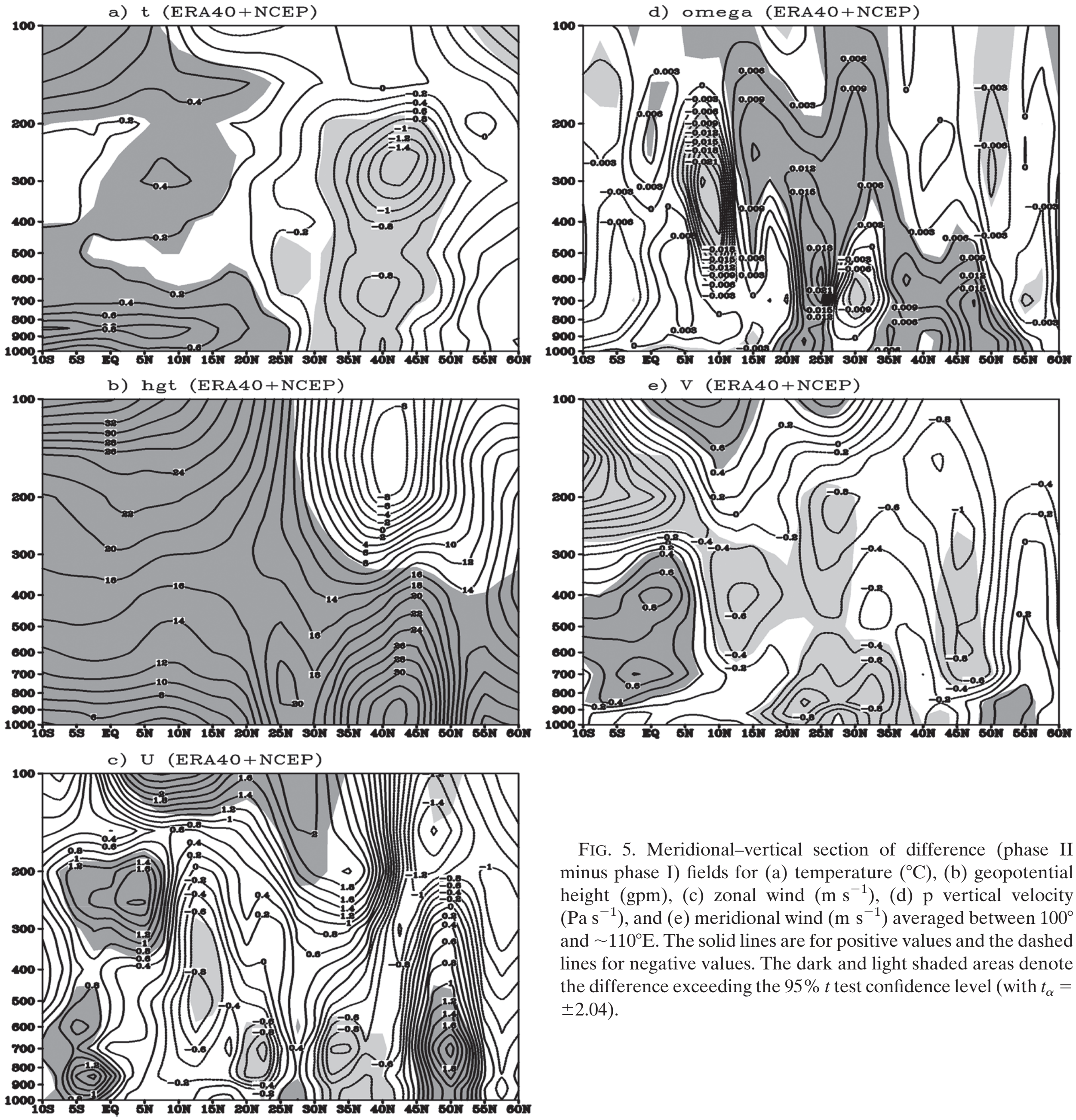

FIG. 5. Meridional–vertical section of difference (phase II minus phase I) fields for (a) temperature (°C), (b) geopotential height (gpm), (c) zonal wind (m s^{-1}), (d) p vertical velocity (Pa s^{-1}), and (e) meridional wind (m s^{-1}) averaged between 100° and ~110°E. The solid lines are for positive values and the dashed lines for negative values. The dark and light shaded areas denote the difference exceeding the 95% t test confidence level (with $t_\alpha = \pm 2.04$).

height anomaly at lower (upper) levels over 30°–50°N (Fig. 5b). The baroclinic geopotential height field results in an anticyclonic (cyclonic) wind anomaly in the lower (upper) troposphere in situ (Fig. 5c). The vertical velocity difference field shows a strong descending branch over the thermal cooling region and a deep convective branch in the equatorial region (10°N–0°) (Fig. 5d). Correspondingly, there are pronounced northerly and easterly wind anomalies in the lower troposphere between 40° and 10°N (Figs. 5c,e).

The midlatitude subsidence may be triggered by either the enhanced equatorial convection or the midlatitude cold temperature perturbation. In the former scenario, the local Hadley circulation or meridional overturning circulation plays a key role. In the latter scenario, the reduced thickness leads to a high (low) pressure anomaly at lower (upper) levels; the pressure gradient further drives divergent (convergent) lower- (upper) level flows and thus local descending motion. A fundamental dynamics question related to the latter scenario is how the cold temperature anomaly is maintained as the induced subsidence may damp the initial temperature perturbation through the adiabatic warming.

An examination of the specific humidity profile sheds light on the question above. Note that there is a significant moisture difference between phases I and II. The water vapor amount decreases throughout the troposphere after 1976 (Fig. 6a). The decrease of the specific humidity is possibly caused by the anomalous low-level divergence and vertical humidity advection as the descending motion brings the dry air downward. As the water vapor is a major greenhouse gas that absorbs the longwave radiation, the decrease of the atmospheric moisture leads to the enhanced outgoing longwave radiation (OLR) into space, which further causes the decrease of the tropospheric temperature.

To validate the argument above, we calculate apparent thermal sources and water vapor sinks (i.e., Q1 and Q2), and the results are shown in Figs. 6b,c. As expected, both vertical-integrated Q1 and Q2 experience an interdecadal change, shifting from positive to negative values, consistent with the decrease of the tropospheric moisture. Thus, the reduction of the atmospheric water vapor, by resulting in a substantial loss of effective longwave radiation and latent heating in the atmosphere, may be responsible for the decrease of the apparent heat sources and thus a cooling in the regional tropospheric temperature.

The argument above implies a local positive feedback between the atmospheric temperature, vertical motion, and moisture over East Asia. On one hand, a cold tropospheric temperature anomaly may induce an upper-level convergence and a lower-level divergence and thus anomalous descending motion. On the other hand, a dryness associated with the subsidence may increase the loss of the atmospheric longwave radiation that offsets the adiabatic warming and leads to the increase of the initial cold temperature anomaly. Through this positive feedback process, the summer temperature and circulation anomalies are maintained.

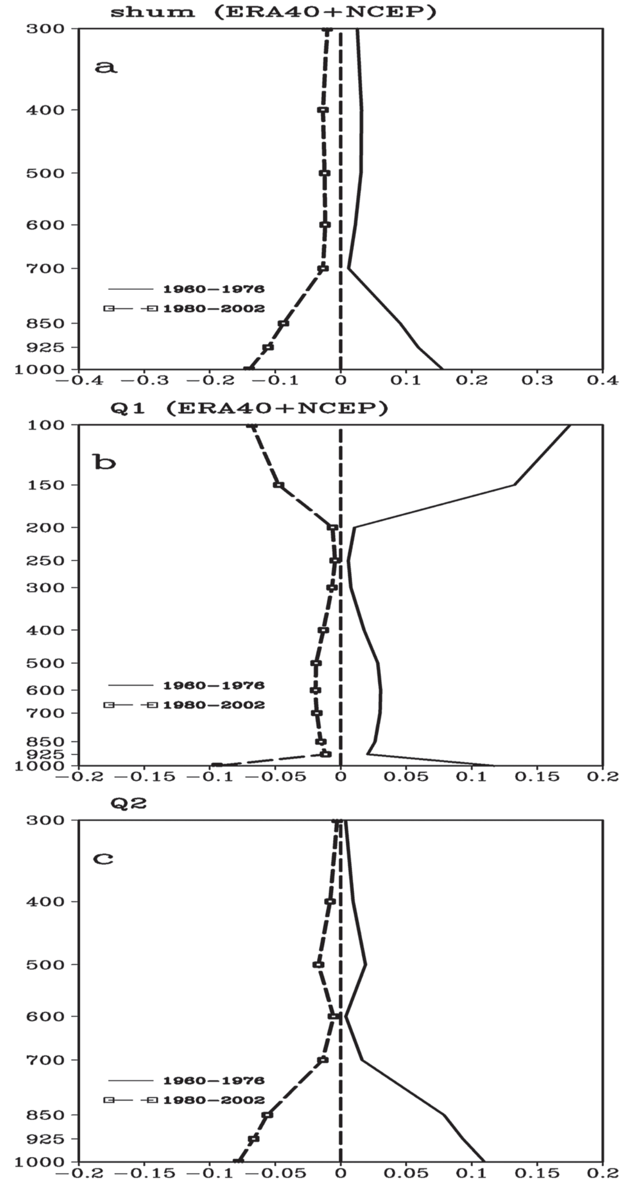

FIG. 6. Vertical profiles of (a) anomalous specific humidity (g kg^{-1}), (b) apparent heat source Q1 (K s^{-1}), and (c) apparent water vapor sink Q2 (K s^{-1}) averaged over 35°∼45°N, 100°∼110°E at phase I (solid line) and phase II (dashed line).

Whereas the previous studies (e.g., Yu and Zhou 2004) suggested the effect of the midlatitude forcing such as NAO in triggering the initial cooling, here we emphasize the tropical forcing. Figure 7 illustrates the OLR difference map and associated meridional overturning circulation composed of 12-layer meridional wind and vertical velocity from 1000 to 100 hPa and averaged over 105°–130°E. Here the OLR field is from NCEP only, as it is not available from ERA-40; all circulation fields are from the NCEP and ERA-40 ensemble mean. The most significant signal in the OLR difference field is an elongated negative OLR anomaly over the southern SCS and WNP region (between 10°N and 0°). This indicates a strengthening convective and ascending branch in the region, as clearly shown in the vertical–meridional section of the difference streamfunction field. The enhanced local Hadley circulation leads to anomalous subsidence in midlatitudes, which may further induce and maintain cold temperature anomalies through the aforementioned positive feedback processes. The anomalous meridional overturning

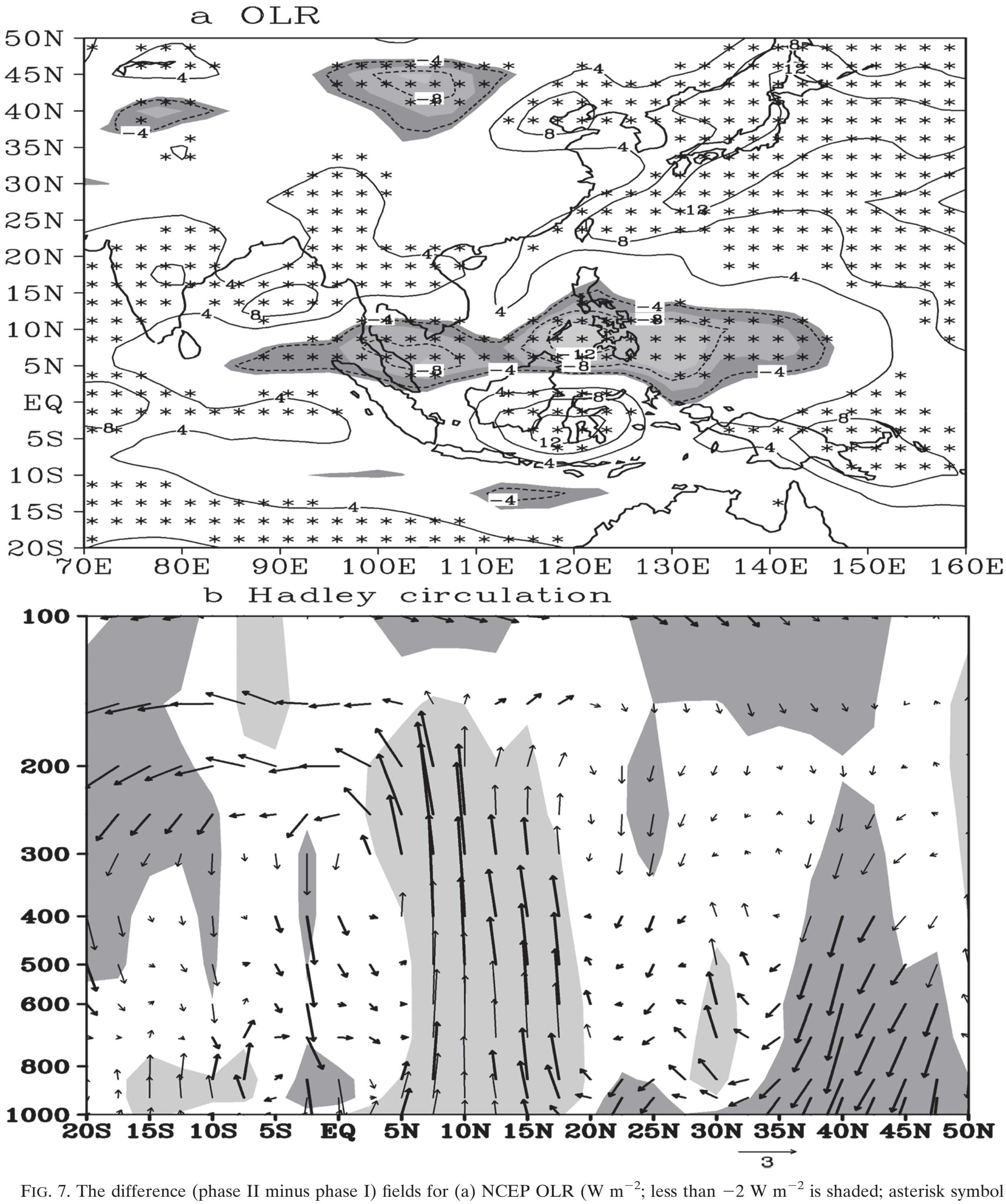

FIG. 7. The difference (phase II minus phase I) fields for (a) NCEP OLR (W m^{-2}; less than -2 W m^{-2} is shaded; asterisk symbol denotes the OLR difference exceeding the 95% t test confidence level with $t_\alpha = \pm 2.04$) and (b) the meridional–vertical streamfunction (from the NCEP and ERA-40 ensemble mean) averaged over 105°–130°E (areas where the meridional and vertical wind differences exceed the 95% confidence level are shaded).

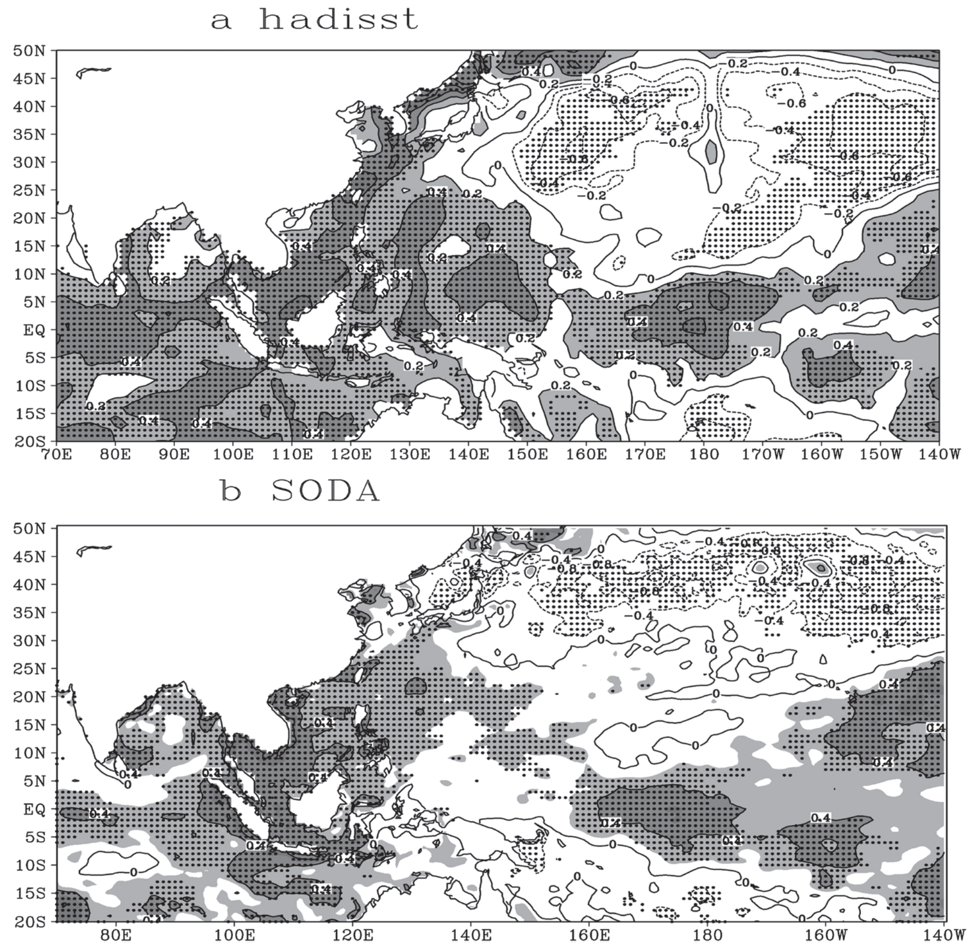

FIG. 8. The summer SST (a) HadISST and (b) SODA (°C) difference (phase II minus phase I) field. The shaded denotes that the SST differences are greater than 0.2° and 0.4°C. Dot symbol denotes the difference exceeding the 95% confidence level (with $t_\alpha = \pm 2.04$).

circulation is also responsible for the weakening of the monsoon southerly over SCS. In addition to forcing the local Hadley circulation, the tropical heating may also excite upper-level Rossby waves that propagate into the higher latitudes.

The strengthened equatorial convection at phase II can possibly be attributed to the warming in the tropical Indian and Pacific Ocean. Figure 8a shows the difference map of the summer HadISST field. Note that the significant warming appears in the Maritime Continent, SCS, and equatorial central Pacific, while a cooling appears in the North Pacific. To examine how sensitive the SST difference field is to different data products, we conduct the same calculation using the global ocean SST field from SODA. The result is shown in Fig. 8b. The gross patterns are similar.

The cause of the warm SSTA in SCS and the cold SSTA in the North Pacific is investigated by analyzing the ensemble-averaged surface latent and sensible heat fluxes and shortwave and longwave radiation anomalies over 10°~20°N, 105°~120°E and 35°~45°N, 140°~180°E. Figure 9 illustrates that the all four heat flux components experienced a significant interdecadal shift in both the regions. In SCS, the net downward shortwave radiation increases after 1976, while the upward latent and sensible heat fluxes and net upward longwave radiation decrease because of the decrease of the local cloud amount and mean wind speed. Thus, all four flux components contribute to the SST change in SCS. The situation is just opposite over the North Pacific. After 1976, the net downward shortwave radiation decreases, while the latent and sensible heat fluxes and the upward longwave radiation increase. It results in a reduced net downward heat flux and causes the ocean surface cooling. Therefore, the interdecadal change of SST in SCS and the North Pacific is, to the first order of approximation, a passive response to the surface heat flux forcing.

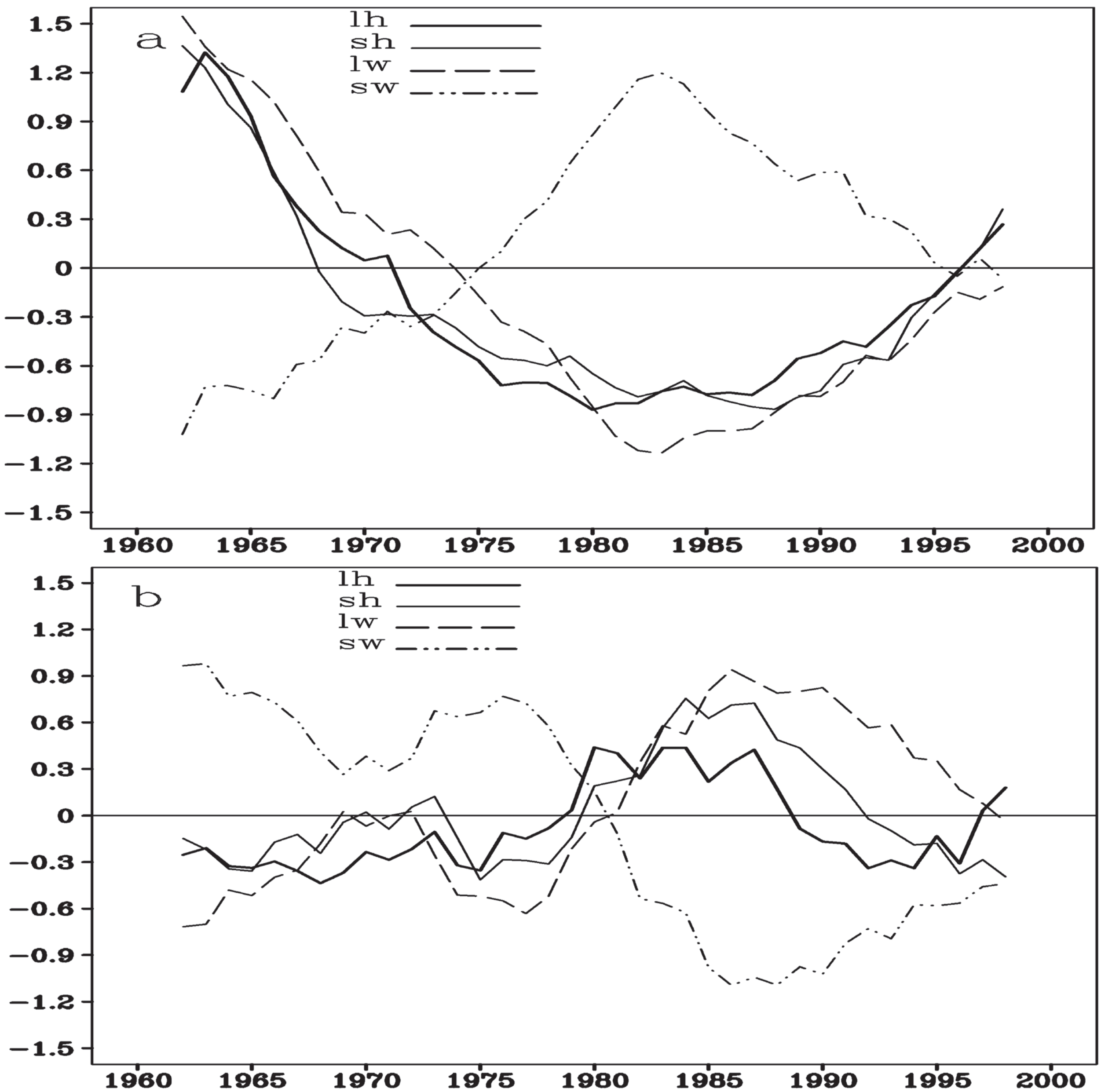

FIG. 9. The 9-yr running mean of the net shortwave radiation (dot dashed line), longwave radiation (dashed line), latent heat flux (thick solid line), and sensible heat flux (thin solid line) from the ensemble average of the NCEP and ERA-40 reanalysis products over (a) the South China Sea (10°–20°N, 105°–120°E) and (b) the North Pacific (35°–45°N, 140°–180°E). The units of the all heat flux terms are W m^{-2}.

4. Relationships between the LLMW in SCS and climate in China

How is the LLMW variation over SCS related to the interannual and interdecadal variability of the summer climate in China? It is likely that the SCS wind may influence the summer rainfall in China through moisture transport. In the following, using the 743 station data across China, we intend to reveal a possible connection between the variations of precipitation and temperature in China and the LLMW over SCS. A time filtering method (i.e., a harmonic analysis) is applied to isolate the interdecadal (longer than 9 yr) and interannual (2–8-yr) time scales.

Figure 10 shows the correlation of the LLMW over SCS with the station rainfall in China for the following three cases. In the first case, both the raw rainfall data and the raw LLMW index are used. In the second case, the raw rainfall data and the interdecadal time series of the LLMW index are used. In the third case, the raw

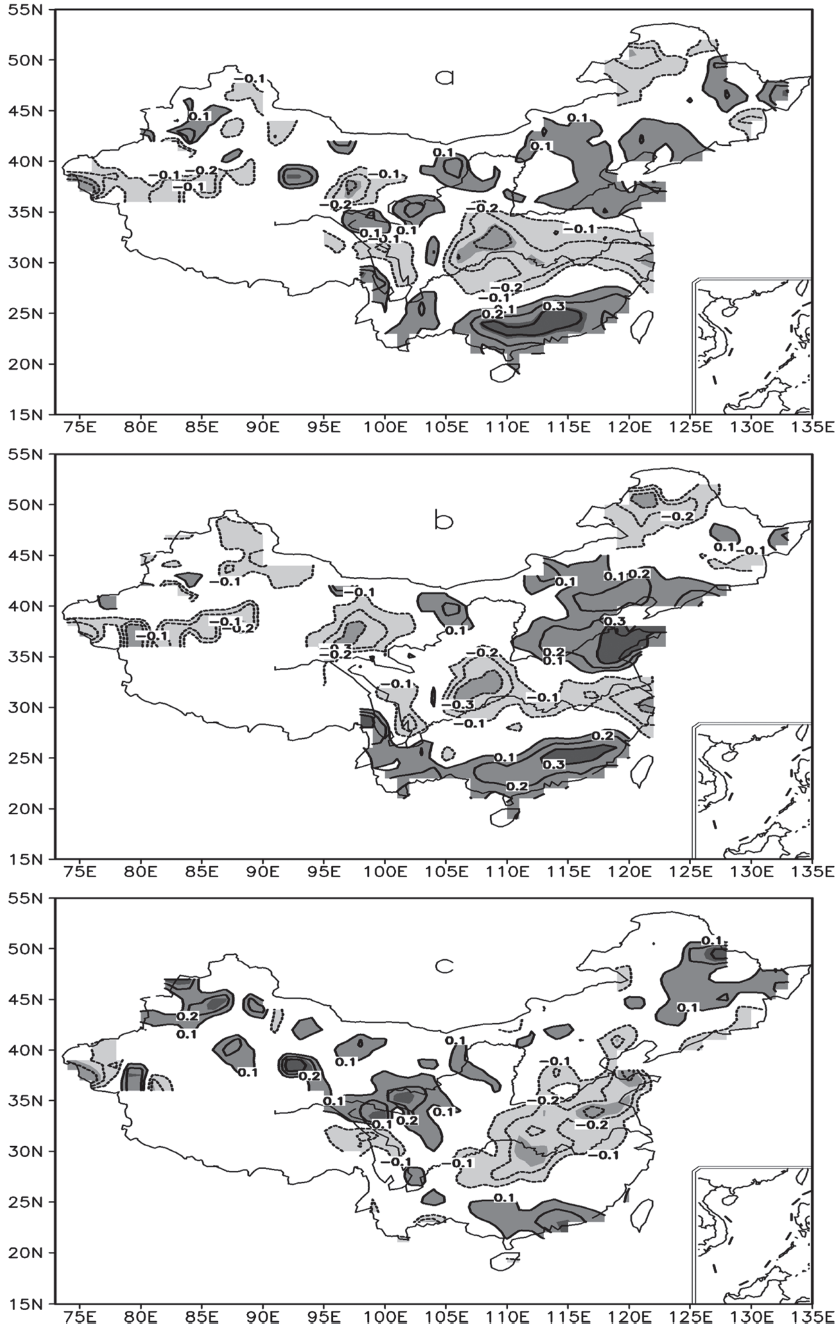

FIG. 10. Distribution of correlations between LLMW and rainfall over the 743 weather stations in China in terms of (a) overall correlation, (b) interdecadal correlation, and (c) interannual correlation. The solid contour (dashed contour) shaded area indicates the correlation coefficient that is larger (less) than 0.1 (−0.1). The darker solid contour (dashed contour) shaded areas denote the positive and negative correlation coefficients that exceed the 90% confidence level. The effective degree of freedom has been taken into account when the significance test is performed. For the raw time series, $r = \pm 0.275$. For the interdecadal time series, $r = \pm 0.296$. For the interannual time series, $r = \pm 0.27$.

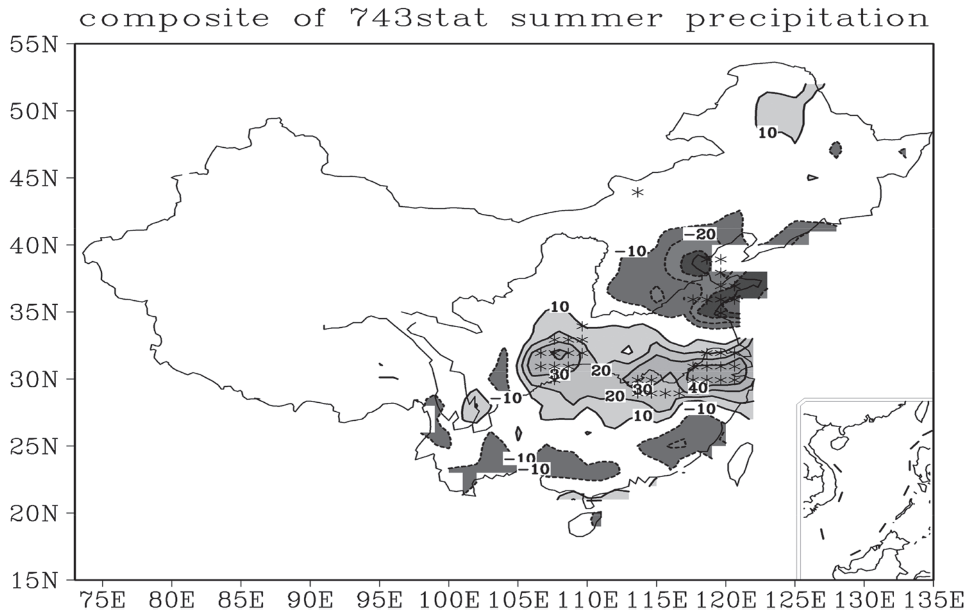

FIG. 11. The difference (Phase II minus Phase I) field of summer precipitation (mm day^{-1}) over the 743 weather stations across China. Asterisk symbol denotes the difference exceeding the 95% t_test confidence level (with $t_\alpha = \pm 2.04$).

rainfall data and the interannual time series of the LLMW index are applied. From Fig. 10a, the most significant positive correlation appears in Guangdong Province, while a negative correlation appears in the Yangtze River valley. This points out that an enhanced LLMW in SCS leads to enhanced precipitation in Guangdong Province and reduced precipitation in the Yangtze River valley. This correlation pattern, as seen from Fig. 10b, is primarily attributed to the interdecadal variability, which differs significantly from the interannual variability in which the LLMW is mainly correlated with rainfall anomalies in Yangtze and Huaihe River valleys (Fig. 10c). Unlike the meridional wind component, the zonal wind in SCS is primarily correlated to the precipitation variability in China on the interannual time scale (figure not shown).

The rainfall difference between phase I and II shows a zonal elongated "−, +, −" pattern (from north to south) with negative anomalies over south China and north China (east of the Yellow River) and positive anomalies over the Yangtze River valley (Fig. 11). While the central and north China rainfall differences exceed the 95% confidence level, the south China rainfall difference just reaches the 90% confidence level. The "−, +, −" rainfall pattern is consistent with the interdecadal LLMW–rainfall correlation map (Fig. 10b).

Compared to the precipitation field, the correlation of the LLMW with the surface air temperature field in China is more pronounced over larger regions (Fig. 12). Again the overall correlation with the raw data has a similar spatial distribution to that on the interdecadal time scale (see left and middle panels of Fig. 12a). Positive correlations are found in the Yangtze and Huaihe River basins and negative correlations are in south and north China. This implies that a weakening of the LLMW leads to a reduction of the air mean temperature in the two river basins and an increase of the air mean temperature in south and north China. This correlation pattern is consistent with the mean temperature (phase II minus phase I) difference map (Fig. 13), except that the correlations in north and northeast China hardly exceed the 95% confidence level. Again, the correlation pattern on the interannual time scale differs from the overall pattern. Significant positive correlations are found only over north China.

The examination of the correlation with maximum and minimum air temperatures (Figs. 12b,c) shows that there is an asymmetry between the maximum and minimum temperatures. While the correlation with the maximum temperature is stronger in the Yangtze and Huaihe River basins and south China and is hardly discerned in north China, the correlation with minimum temperature is significantly negative over northeast and northwest China. In other words, when the LLMW over SCS is weakening, the minimum temperature is rising over northeast and northwest China. The overall correlation patterns confirm that the LLMW variation over SCS is primarily related to the interdecadal climate change in China.

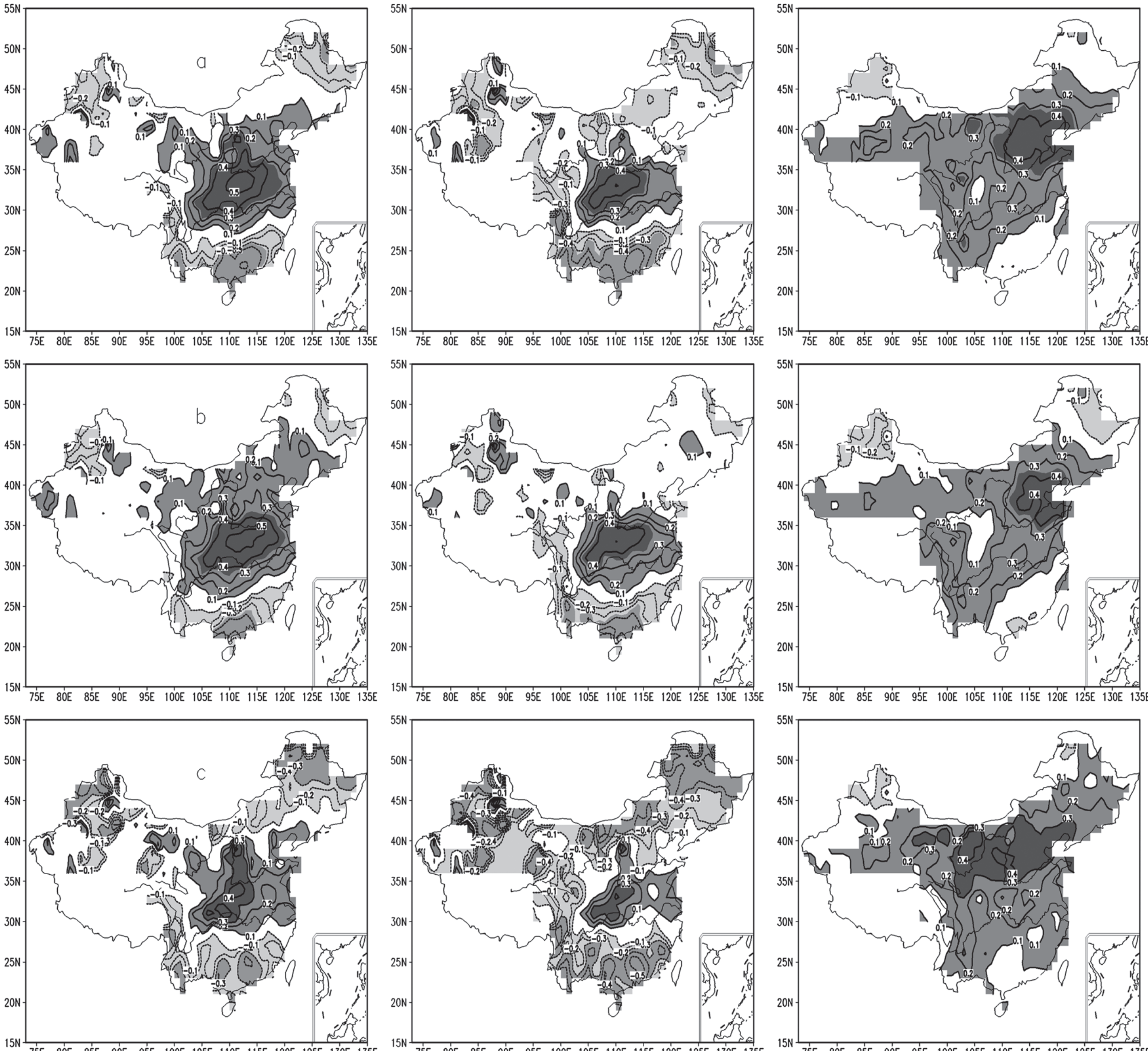

FIG. 12. Distribution of correlations between LLMW and (a) mean temperature, (b) maximum temperature, and (c) minimum temperature over the 743 weather stations in China. The left panel is for the overall correlation with raw temperature data, the middle panel for the interdecadal correlation and the right panel for the interannual correlation. The solid contour (dashed contour) shaded area indicates the correlation coefficient larger (less) than 0.1 (-0.1). The darker solid contour (dashed contour) shaded area denotes the positive and negative correlation coefficients that exceed the 95% confidence level. For the raw temperature data, $r = \pm 0.325$. For the interdecadal time series, $r = \pm 0.349$. For the interannual time series, $r = \pm 0.27$.

5. Conclusions and discussion

Both the NCEP and ERA-40 reanalysis products and the Xisha Island station observation reveal that the low-level meridional wind (LLMW) over the SCS experienced an interdecadal variation since the late 1970s. The LLMW change is associated with the large-scale temperature and circulation change in East Asia.

The reduction of the tropospheric temperature in midlatitude East Asia has been documented, and it was argued to be mainly related to the NAO forcing (Yu and Zhou 2004, 2007; Li et al. 2005). A new hypothesis is put forward here in which the tropical forcing is crucial. The enhanced convective heating over the southern SCS (associated with the equatorial Indian and Pacific Ocean warming) may result in a meridional overturning circulation over the East Asian longitudes. This leads to anomalous descending motion over continental East Asia. In summer, the mean ascending motion appears over the East Asian monsoon region. Thus the anomalous descending

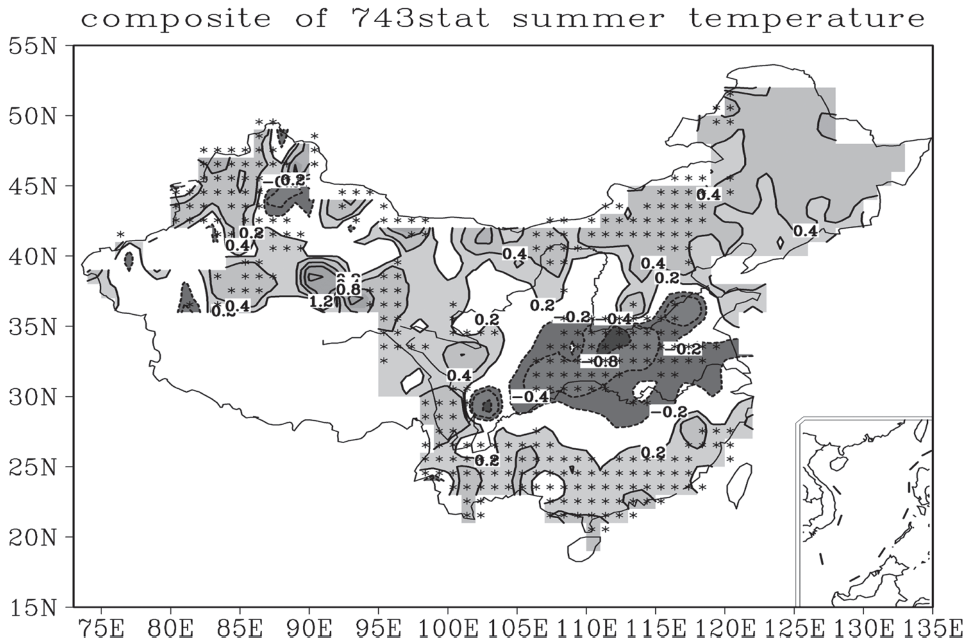

FIG. 13. The difference (Phase II minus Phase I) field of summer mean temperature (°C) over the 743 weather stations across China. Symbol * denotes the difference exceeding the 95% t_test confidence level (with $t_\alpha = \pm 2.04$).

motion may reduce the moisture flux convergence into the East Asian land region. The vertical humidity advection due to the anomalous descending motion also brings dry air downward. Both the processes above cause the decrease of local moisture throughout the troposphere. The decrease of vertical-integrated humidity leads to the enhanced outgoing longwave radiation into space, and as a result the tropospheric temperature drops. The decrease of the tropospheric temperature (and thickness) leads to the low (high) pressure anomaly and thus convergent (divergent) flows at upper (lower) levels, the latter of which further enhances the local descending motion induced by the tropical heating. The enhanced subsidence further reduces the water vapor and strengthens the tropospheric cooling and upper-(lower) level convergence (divergence).

The argument above points out a local positive feedback process, under which either an initial anomalous cooling or downward motion triggered by external forcing may reinforce each other. Figure 14 is a schematic diagram illustrating the positive feedback process. Suppose that initially there is anomalous descending motion over the continental East Asia due to strengthened tropical heating. The descending motion leads to the decrease of the local moisture and thus the increase of outgoing longwave radiation into space. This diabatic process overcomes the effect of adiabatic warming and leads to the tropospheric cooling. The cooling has two effects. First, its hydrostatic effect leads to the decrease of thickness and thus negative (positive) geopotential height anomalies and anomalous convergent (divergent) flows in the upper (lower) troposphere. Secondly, it leads to a reduced land–sea thermal contrast and thus the weakening of the southerly flow and northward moisture transport, the latter of which further weakens the East Asian monsoon strength. Both of the processes above enhance the local subsidence over East Asia. The enhanced downward motion may lead to further amplification of the temperature and circulation anomalies, and therefore a positive feedback loop goes on.

This positive feedback mechanism explains why the observed atmospheric temperature and circulation anomalies may persist throughout the entire summer season until the background mean state over the continental East Asia changes from a wet to a dry condition. The tropospheric cooling over East Asia reduces the land–sea thermal contrast and is responsible for the weakening of cross-equatorial flows and the LLMW over SCS.

Our diagnosis indicates that the warming of SST over SCS in the recent decadal period (at phase II) results from the combined effect of a decrease in the surface latent and sensible heat fluxes and longwave radiative fluxes and an increase in downward shortwave radiative fluxes. This indicates that the ocean takes heat from the

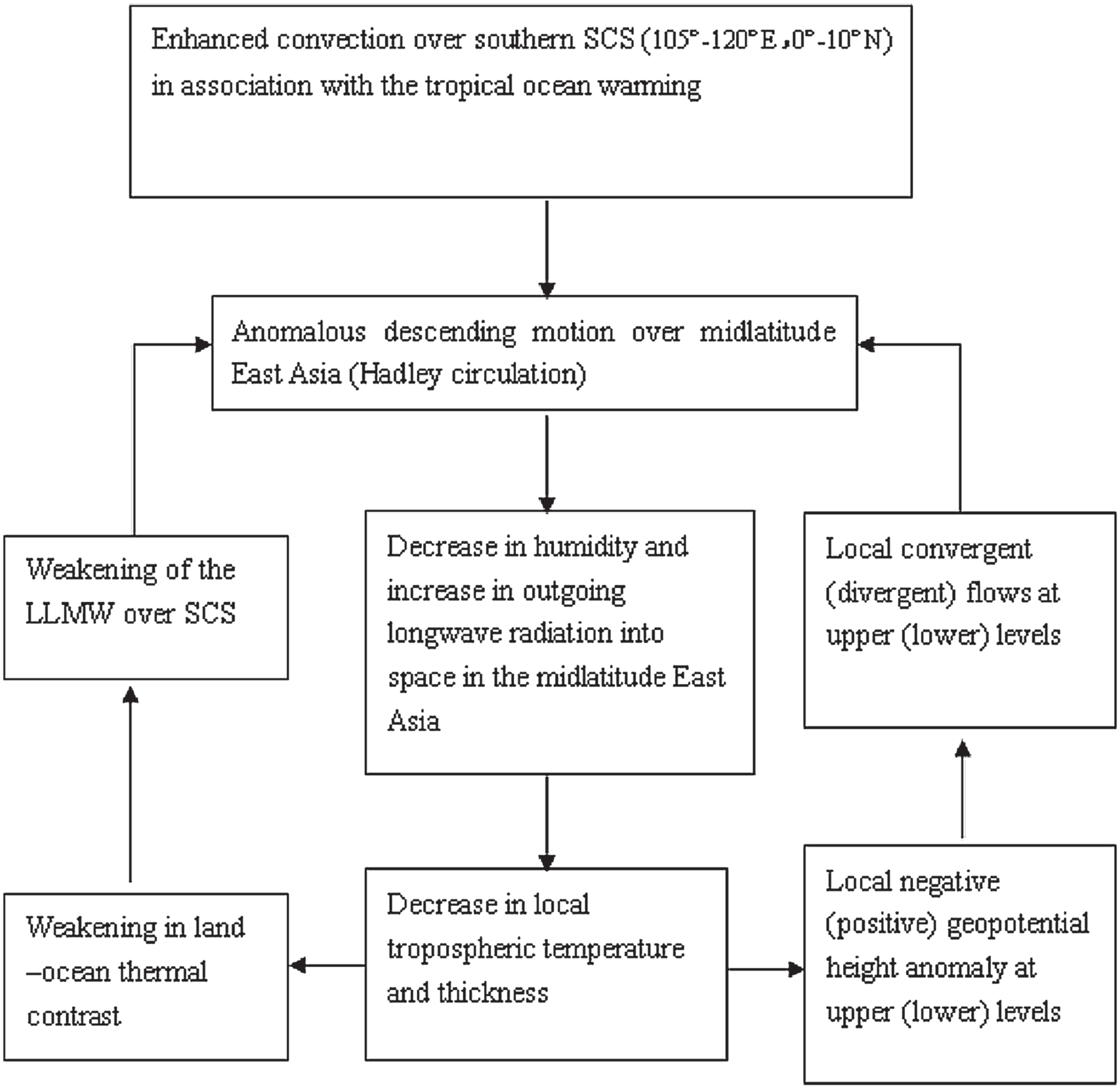

FIG. 14. A schematic diagram illustrating a positive feedback among the local descending motion, humidity, outgoing longwave radiation, and tropospheric cooling over the midlatitude East Asia in boreal summer.

atmosphere. This is in contrast to the interdecadal SST change over North Pacific, where an increase in latent and sensible heat fluxes and longwave radiation and a decrease in downward shortwave radiation account for the ocean cooling, indicating that it is the ocean that gives heat to the atmosphere in the region.

By separating the interannual and interdecadal time scales, we note that the LLMW over SCS is significantly linked to the climate variation in China on the interdecadal scale. The LLMW is correlated with a meridional "−, +, −" precipitation pattern in which there is less rain in Guangdong Province and north China but more rain in the Yangtze and Huaihe River basins. In addition, the LLMW over SCS is also associated with the mean temperature tripole pattern, with a positive (negative) temperature anomaly located in south and northeast/northwest (central) China. For the maximum temperature, significant positive (negative) correlations are found in central (south) China. For the minimum temperature, significant correlations are found in north and northeast China and the Xinjiang region, which leads to a "−, +, −" meridional pattern, with the minimum temperature rising (falling) in the south and north (central) China since 1976.

It was reported that the NCEP reanalysis data may have some problems prior to 1968 (Yang et al. 2002). To examine whether this may affect our major conclusions, we conducted a parallel analysis in which for phase I only the period of 1968–76 is used for the NCEP data while keeping the same analysis period for the ERA-40 data. It turns out that the major conclusions derived from the current study do not change.

Acknowledgments. This work was supported by the National Basic Research Program of China (2006CB403600), National Natural Science Foundation of China (90211010, 40775058, 40675054, 40675055, and 40505019), Natural Science Foundation of Guangdong (06020745), and China Meteorological Administration under Contract CMATG2006L03. TL was supported by ONR Grants N000140710145 and N000140810256 and by the International Pacific Research Center that is sponsored by the Japan Agency for Marine-Earth Science and Technology (JAMSTEC), NASA (NNX07AG53G), and NOAA (NA17RJ1230).

REFERENCES

Carton, J. A., and B. S. Giese, 2008: A reanalysis of ocean climate using Simple Ocean Data Assimilation (SODA). *Mon. Wea. Rev.,* **136,** 2999–3017.

Chang, C.-P., Y. Zhang, and T. Li, 2000a: Interannual and interdecadal variations of the East Asian summer monsoon and tropical Pacific SSTs. Part I: Roles of the subtropical ridge. *J. Climate,* **13,** 4310–4325.

——, ——, and ——, 2000b: Interannual and interdecadal variations of the East Asian summer monsoon and tropical Pacific SSTs. Part II: Meridional structure of the monsoon. *J. Climate,* **13,** 4326–4340.

Chen, J.-H., and L.-X. Chen, 1991: Influence of ocean–continent distribution in the south part of Asia on the formation of Asian summer monsoon (in Chinese). *J. Appl. Meteor. Sci.,* **2,** 355–361.

Dai, N.-J., A. Xie, and Y. Zhang, 2000: Interannual and interdecadal variations of summer monsoon activities over South China Sea (in Chinese). *Climate Environ. Res.,* **5,** 363–374.

Guo, Q.-Y., J.-N. Cai, X.-M. Shao, and W.-Y. Sha, 2003: Interdecadal variability of East-Asian summer monsoon and its impact on the climate of China (in Chinese). *Acta Geogr. Sin.,* **58,** 569–576.

Huang, G., 1999: Study on the relationship between summer monsoon circulation anomaly index and the climatic variation in East Asia (in Chinese). *J. Appl. Meteor. Sci.,* **10,** 61–69.

Huang, R.-H., 2001: Decadal variability of the summer monsoon rainfall in East Asia and its association with the SST anomalies in the tropical Pacific. *CLIVAR Exchanges,* No. 2, International CLIVAR Project Office, Southampton, United Kingdom, 7–8.

——, Y.-H. Xu, and L.-T. Zhou, 1999: The interdecadal variation of summer precipitation in China and the drought trend in north China (in Chinese). *Plateau Meteor.,* **18,** 465–475.

Lanzante, J., 1996: Lag relationships involving tropical sea surface temperatures. *J. Climate,* **9,** 2568–2578.

Li, C.-Y., and L.-P. Zhang, 1999: Summer monsoon activities in the South China Sea and their impacts (in Chinese). *Chin. J. Atmos. Sci.,* **23,** 257–266.

——, G.-L. Li, and Z.-X. Long, 1999: Comparing analyses of atmospheric circulation for interdecadal climate variation in China (in Chinese). *J. Appl. Meteor. Sci.,* **10** (s1), 1–8.

Li, F., and J.-H. He, 2001: Study on interdecadal relation features of north Pacific SSTA with East Asian summer monsoon as well as its mechanism (in Chinese). *J. Nanjing Inst. Meteor.,* **24,** 199–206.

Li, J., R.-C. Yu, T.-J. Zhou, and B. Wang, 2005: Why is there an early spring cooling shift downstream of the Tibetan Plateau? *J. Climate,* **18,** 4660–4668.

Liang, J.-Y., and S.-S. Wu, 2003: Diagnostic analysis of interdecadal change of the summer monsoon in the South China Sea (in Chinese). *Acta Meteor. Sin.,* **7** (s1), 81–94.

——, S. Yang, C.-H. Li, and X. Li, 2007: Long-term changes in the South China Sea summer monsoon revealed by station observations of the Xisha Islands. *J. Geophys. Res.,* **112,** D10104, doi:10.1029/2006JD007922.

Magaritz, M., and G. A. Goodfriend, 1987: Movement of the desert boundary in the Levant from latest Pleistocene to early Holocene. *Abrupt Climatic Change: Evidence and Implications,* W. H. Berger and L. D. Labeyrie, Eds., NATO ASI Series C: Mathematical and Physical Sciences, Vol. 216, Kluwer Academic, 173–183.

Murakami, T., 1959: The general circulation and water vapor balance over the Far East during the rainy season. *Geophys. Mag.,* **29,** 131–171.

Nitta, T., and S. Yamada, 1989: Recent warming of tropical sea surface temperature and its relationship to Northern Hemisphere circulation. *J. Meteor. Soc. Japan,* **67,** 375–383.

Rayner, N. A., D. E. Parker, E. B. Horton, C. K. Folland, L. V. Alexander, D. P. Rowell, E. C. Kent, and A. Kaplan, 2003: Global analyses of sea surface temperature, sea ice and night marine air temperature since the late nineteenth century. *J. Geophys. Res.,* **108,** 4407, doi:10.1029/2002JD002670.

Ren, X.-J., and Y.-F. Qian, 2003: Numerical simulation experiment of the impacts of local land–sea thermodynamic contrasts on the SCS summer monsoon onset (in Chinese). *J. Trop. Meteor.,* **18,** 327–334.

Shen, S., and K.-M. Lau, 1995: Biennial oscillation associated with the East Asian summer monsoon and tropical sea surface temperature. *J. Meteor. Soc. Japan,* **73,** 105–124.

Sun, X.-R., L.-X. Chen, and J.-H. He, 2002: Index of land–sea thermal difference and its relation to interannual variation of summer circulation and rainfall over East Asia (in Chinese). *Acta Meteor. Sin.,* **60,** 164–172.

Tomita, T., and T. Yasunari, 1996: Role of the northeast winter monsoon on the biennial oscillation of the ENSO/monsoon system. *J. Meteor. Soc. Japan,* **74,** 399–413.

Wang, B., 1995: Interdecadal changes in El Niño onset in the last four decades. *J. Climate,* **8,** 267–285.

——, R. Wu, and X. Fu, 2000: Pacific–East Asia teleconnection: How does ENSO affect East Asian climate? *J. Climate,* **13,** 1517–1536.

Wang, H.-J., 2001: The weakening of the Asian monsoon circulation after the end of 1970's. *Adv. Atmos. Sci.,* **18,** 376–386.

——, 2002: Instability of the East Asian summer monsoon–ENSO relation. *Adv. Atmos. Sci.,* **19,** 1–11.

Xin, X.-G., R.-C. Yu, T.-J. Zhou, and B. Wang, 2006: Drought in late spring of south China in recent decades. *J. Climate,* **19,** 3197–3206.

Yang, S., K.-M. Lau, and K.-M. Kim, 2002: Variations of the East Asian jet stream and Asian–Pacific–American winter climate anomalies. *J. Climate,* **15,** 306–325.

Yu, R.-C., and T.-J. Zhou, 2004: Impacts of winter-NAO on March cooling trends over subtropical Eurasia continent in the recent half century. *Geophys. Res. Lett.,* **31,** L12204, doi:10.1029/2004GL019814.

——, and ——, 2007: Seasonality and three-dimensional structure of the interdecadal change in East Asian monsoon. *J. Climate,* **20,** 5344–5355.

——, B. Wang, and T.-J. Zhou, 2004: Tropospheric cooling and summer monsoon weakening trend over East Asia. *Geophys. Res. Lett.,* **31,** L22212, doi:10.1029/2004gl021270.

Zeng, Z.-M., and Z.-W. Yan, 1999: Analysis on the significance of global warming trends during the last 100 years (in Chinese). *J. Appl. Meteor. Sci.,* **10** (s1), 23–33.

——, ——, and D.-Y. Ye, 2001: The regions with the most significant temperature trends during the last century. *Adv. Atmos. Sci.,* **18,** 481–496.

Zhou, T.-J., and R.-C. Yu, 2005: Atmospheric water vapor transport associated with typical anomalous summer rainfall patterns in China. *J. Geophys. Res.,* **110,** D08104, doi:10.1029/2004JD005413.